



HAL
open science

Loci of extrema of thermodynamic response functions for the Lennard-Jones fluid

Claudio Cerdeiriña, Pablo Téllez-Arredondo, Milton Medeiros, Manuel Piñero

► **To cite this version:**

Claudio Cerdeiriña, Pablo Téllez-Arredondo, Milton Medeiros, Manuel Piñero. Loci of extrema of thermodynamic response functions for the Lennard-Jones fluid. *Molecular Physics*, 2011, 109 (20), pp.2443-2449. 10.1080/00268976.2011.619505 . hal-00743045

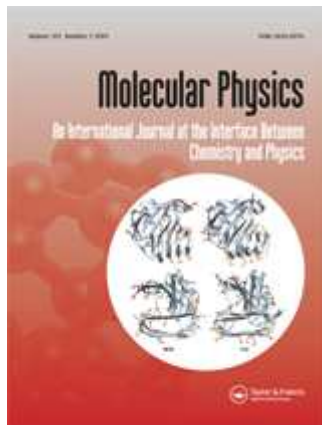
HAL Id: hal-00743045

<https://hal.science/hal-00743045>

Submitted on 18 Oct 2012

HAL is a multi-disciplinary open access archive for the deposit and dissemination of scientific research documents, whether they are published or not. The documents may come from teaching and research institutions in France or abroad, or from public or private research centers.

L'archive ouverte pluridisciplinaire **HAL**, est destinée au dépôt et à la diffusion de documents scientifiques de niveau recherche, publiés ou non, émanant des établissements d'enseignement et de recherche français ou étrangers, des laboratoires publics ou privés.



Loci of extrema of thermodynamic response functions for the Lennard-Jones fluid

Journal:	<i>Molecular Physics</i>
Manuscript ID:	TMPH-2011-0267.R1
Manuscript Type:	Full Paper
Date Submitted by the Author:	21-Aug-2011
Complete List of Authors:	Cerdeiriña, Claudio; Universidad de Vigo, Departamento de Física Aplicada Téllez-Arredondo, Pablo; Universidad Nacional Autónoma de México, Departamento de Físicoquímica Medeiros, Milton; Universidad Nacional Autónoma de México, Departamento de Físicoquímica Piñeiro, Manuel; Universidad de Vigo, Departamento de Física Aplicada
Keywords:	thermodynamic response functions, loci of extrema, Lennard-Jones fluid
<p>Note: The following files were submitted by the author for peer review, but cannot be converted to PDF. You must view these files (e.g. movies) online.</p>	
Source files.zip	

SCHOLARONE™
Manuscripts

1
2
3
4
5
6
7
8
9
10
11
12
13
14
15
16
17
18
19
20
21
22
23
24
25
26
27
28
29
30
31
32
33
34
35
36
37
38
39
40
41
42
43
44
45
46
47
48
49
50
51
52
53
54
55
56
57
58
59
60

For Peer Review Only

FULL PAPER**Loci of extrema of thermodynamic response functions
for the Lennard-Jones fluid**Pablo Téllez-Arredondo,^a Milton Medeiros^aManuel M. Piñeiro,^b and Claudio A. Cerdeiriña^b^aDepartamento de Físicoquímica, Facultad de Química, Universidad Nacional Autónoma de México, Ciudad de México 04510, Mexico^bDepartamento de Física Aplicada, Universidad de Vigo – Campus del Mar, As Lagoas s/n, 32004 Ourense, Spain

1
2
3
4
5
6
7
8
9
10
11
12
13
14
15
16
17
18
19
20
21
22
23
24
25
26
27
28
29
30
31
32
33
34
35
36
37
38
39
40
41
42
43
44
45
46
47
48
49
50
51
52
53
54
55
56
57
58
59
60

Loci of extrema of thermodynamic response functions for the Lennard-Jones fluid

Abstract

Lines of extrema along isotherms and isobars for the residual isochoric heat capacity, the residual isobaric heat capacity, the isobaric thermal expansivity, and the isothermal compressibility of the Lennard-Jones fluid have been studied from popular equations of state due to Johnson et al. [Mol. Phys. **78**, 591 (1993)], Kolafa and Nezbeda [Fluid Phase Equilib. **100**, 1 (1994)], and Mecke et al. [Int. J. Thermophys. **17**, 391 (1996)]. On depicting such loci in the pressure-temperature plane, the characteristic behavior of thermodynamic response functions in the ideal-gas limit (at high enough temperatures or low enough pressures), the close-packed-fluid limit (at low enough temperatures or high enough pressures) as well as in the liquid and critical regions is identified. The present analysis is informative itself, but it also stimulates further work in order to tackle more complicated cases of study including associated fluids like alcohols and low-temperature water.

Keywords: thermodynamic response functions; loci of extrema; Lennard-Jones fluid

1. Introduction

In 1965 Rowlinson asserted [1] that the thermodynamic properties of the fluid phases of simple substances can be conveniently mapped by considering the lines in p - V - T space along which important derivatives vanish. He exposed the experimental situation for the so-called Brown characteristic curves [2], namely, the Amagat (or Joule inversion), Boyle, and Charles (or Joule-Thomson inversion) lines, defined, respectively, by Equations (1) to (3) below:

$$(\partial Z / \partial T)_V = 0, \quad (1)$$

$$(\partial Z / \partial V)_T = 0, \quad (2)$$

$$(\partial Z / \partial T)_p = 0, \quad (3)$$

where $Z \equiv pV / RT$ is the compressibility factor. Two further lines of second-order derivatives or thermodynamic response functions were mentioned: from

$$(\partial C_V^{res} / \partial V)_T = 0 \Leftrightarrow (\partial C_V^{res} / \partial p)_T = 0, \quad (4)$$

$$(\partial C_p^{res} / \partial V)_T = 0 \Leftrightarrow (\partial C_p^{res} / \partial p)_T = 0, \quad (5)$$

one gets loci of extrema for the residual isochoric and isobaric heat capacities, $C_V^{res} \equiv C_V - C_V^{ig}$ and $C_p^{res} \equiv C_p - C_p^{ig}$ (superscript “ig” denotes property in the ideal-gas state), along a path of constant temperature, that is, they are loci of isothermal extrema.

As it has been emphasized recently in connection with the Amagat line [3], calculation of the above loci is highly demanding for equations of state (EoS). Moreover, since adequate representation of thermodynamic response functions constitutes a stringent test for EoS [4], it may not be surprising that much care must be taken when

dealing with loci defined by Equations (4) and (5). Such a task was undertaken by Stephenson [5-14], who, in addition to Brown's characteristic curves and the line defined by Equation (4), studied the loci of isobaric extrema of the isobaric thermal expansivity α_p , given by

$$(\partial\alpha_p/\partial V)_p = 0 \Leftrightarrow (\partial\alpha_p/\partial T)_p = 0. \quad (6)$$

Here we report calculations of the isothermal and isobaric lines of extrema for C_V^{res} , C_p^{res} , α_p , and for the isothermal compressibility κ_T of the Lennard-Jones (LJ) fluid. To this end, the widely known EoS by Johnson et al. [15], Kolafa and Nezbeda [16], and Mecke et al. [17] were employed. Our results complement those by Stephenson on two counts: (i) they have been obtained on the solid basis of correlating EoS for a complete set of simulation data for the Lennard-Jones fluid and (ii) the study is extended to unexplored-to-date lines, defined from

$$(\partial C_V^{res}/\partial V)_p = 0 \Leftrightarrow (\partial C_V^{res}/\partial T)_p = 0, \quad (7)$$

$$(\partial C_p^{res}/\partial V)_p = 0 \Leftrightarrow (\partial C_p^{res}/\partial T)_p = 0, \quad (8)$$

$$(\partial\alpha_p/\partial V)_T = 0 \Leftrightarrow (\partial\alpha_p/\partial p)_T = 0, \quad (9)$$

$$(\partial\kappa_T/\partial V)_T = 0 \Leftrightarrow (\partial\kappa_T/\partial p)_T = 0, \quad (10)$$

$$(\partial\kappa_T/\partial V)_p = 0 \Leftrightarrow (\partial\kappa_T/\partial T)_p = 0. \quad (11)$$

Results, as graphically represented in the regions of the $p-T$ plane corresponding to the stable fluid phases, are found to be relevant themselves, but also with a view to extend calculations to associated fluids including the study of water at low temperatures.

2. Equations of state for the Lennard-Jones fluid

The three equations of state employed provide an expression for the residual Helmholtz energy A_{res} as a function of temperature T and number density $\rho \equiv N/V$ (N is the number of particles). For convenience, variables will be made dimensionless: $T^* \equiv Tk_B / \varepsilon$, $\rho^* \equiv \rho\sigma^3$, $p^* \equiv p\sigma^3 / \varepsilon$, and $A_{res}^* = A_{res}/N\varepsilon$, where ε and σ are the LJ characteristic parameters (well depth and atomic diameter) while k_B is the Boltzmann constant.

In 1993 Johnson et al. [15] presented a comprehensive set of simulation data for the LJ fluid and used them to improve a modified Benedict-Webb-Rubin (MBWR) equation of state, previously used by Nicolas et al. [18]. The corresponding residual Helmholtz energy for this MBWR EoS, which has 33 adjustable parameters, is given by:

$$A_{res}^* = \sum_{i=1}^8 \frac{a_i(T^*)\rho^{*i}}{i} + \sum_{i=1}^6 b_i(T^*)G_i(\rho^*). \quad (12)$$

The explicit functional forms of $a_i(T^*)$, $b_i(T^*)$, and $G_i(\rho^*)$ can be found in the original paper. This equation provides an accurate correlation of pressure and internal energy from the triple point to $4.5T_c$ (where T_c denotes the critical temperature).

A year later, in 1994, Kolafa and Nezbeda [16] developed a 20-parameter EoS based on a perturbed virial expansion (PVE) with a theoretically defined reference hard sphere term. They employed the hybrid Barker-Henderson (hBH) perturbation theory, giving rise to the following expression for the residual Helmholtz energy:

$$A_{res}^* = A_{HS}^* + \exp(-\gamma\rho^{*2})\rho^*T^*\Delta B_{2,hBH} + \sum_{ij} C_{ij}T^{*i/2}\rho^{*j}, \quad (13)$$

where

$$A_{HS}^* = T^* \left[\frac{5}{3} \ln(1 - \eta) + \frac{\eta(34 - 33\eta + 4\eta^2)}{6(1 - \eta)^2} \right], \quad (14)$$

$$\eta = \frac{\pi \rho^* d_{hBH}^3}{6}, \quad (15)$$

$$d_{hBH} = \sum_i C_i T^{*i/2} + C_{ln} \ln(T^*), \quad (16)$$

$$\Delta B_{2,hBH} = \sum_i C_i T^{*i/2}. \quad (17)$$

The first two terms in Equation (13) correspond to the perturbed virial expansion while the last one is a small empirical correction term, A_{HS}^* is the hard sphere Helmholtz energy from Boublík and Nezbeda [19], η is the packing fraction, d_{hBH} is the temperature-dependent hard sphere diameter, $\Delta B_{2,hBH}$ is the residual second virial coefficient, and i and j are specific exponents. Values for the (constant) coefficients γ , C_{ij} , C_i , C_{ln} , and the exponents i and j can be found in the original paper. Kolafa and Nezbeda's EoS, termed PVE/hBH, can be employed from the triple point up to $7T_c$. It provides very accurate predictions for compressibility, internal energy, chemical potential, second virial coefficient, and properties at vapor-liquid coexistence.

Then, in 1996 Mecke et al. [17] proposed a generalized Van der Waals-type equation of state, henceforth to be referred to as VdW-LJ, which uses 32 adjustable parameters. Concretely:

$$\begin{aligned} A_{res}^* &= A_{HS}^* + A_{ADF}^* \\ &= T^* \frac{4\xi - 3\xi^2}{(1 - \xi)^2} + T^* \sum_i c_i (T^*/T_c^*)^{m_i} (\rho^*/\rho_c^*)^{n_i} \exp[p_i (\rho^*/\rho_c^*)^{q_i}], \end{aligned} \quad (18)$$

where A_{HS}^* is the hard sphere Helmholtz energy due to Carnahan and Starling [20], ξ is the packing fraction from Saager et al. [21] correlation ($\xi = 0.1617(\rho^*/\rho_c^*)[0.689 + 0.311(T^*/T_c^*)^{0.3674}]^{-1}$), A_{ADF}^* is the Helmholtz energy of the attractive dispersive forces,

T_c^* and ρ_c^* are the dimensionless critical temperature and density, respectively, and m_i , n_i , p_i , q_i and c_i are adjustable parameters (see Refs. 17 and 22). This EoS covers the whole fluid region up to the highest densities from the triple point up to $T^* = 10$, producing very accurate results for pressure, internal energy, second and third virial coefficients, enthalpy of vaporization and properties at vapor-liquid coexistence.

3. Calculation of loci of extrema

To get explicit results, we first obtain the pressure from $p = -(\partial A / \partial V)_{T,N}$, where

$A = A_{ig} + A_{res}$. In dimensionless form,

$$p^* = \rho^* T^* + \rho^{*2} \left(\frac{\partial A_{res}^*}{\partial \rho^*} \right)_{T^*}. \quad (19)$$

Thermodynamic derivatives are determined using standard thermodynamic relations.

Hence, for the dimensionless isothermal compressibility $\kappa_T^* \equiv \kappa_T \varepsilon / \sigma^3$ and isobaric

thermal expansivity $\alpha_p^* \equiv \alpha_p \varepsilon / k_B$ we find

$$\kappa_T^* = \frac{1}{\rho^*} \left(\frac{\partial p^*}{\partial \rho^*} \right)_{T^*}^{-1}, \quad (20)$$

$$\alpha_p^* = \left(\frac{\partial p^*}{\partial T^*} \right)_{\rho^*} \kappa_T^*. \quad (21)$$

The dimensionless isochoric residual heat capacity per particle $C_V^{res*} \equiv C_V^{res} / Nk_B$ is

obtained via

$$C_V^{res*} = -T^* \left(\frac{\partial^2 A_{res}^*}{\partial T^{*2}} \right)_{\rho^*}, \quad (22)$$

which together with α_p^* and κ_T^* yields the dimensionless isobaric residual heat capacity

per particle $C_p^{res*} \equiv C_p^{res} / Nk_B$:

$$C_p^{res*} = C_V^{res*} + \frac{T^*}{\rho^*} \frac{\alpha_p^{*2}}{\kappa_T^*} - 1. \quad (23)$$

Derivatives are calculated numerically with the aid of Ridders' method [23].

The procedure to calculate loci of extrema for a given thermodynamic response function X is as simple as follows. For the isothermal case we fix the temperature and calculate $X(p)$. Then, extrema are determined from first and second-order derivatives, which are calculated using Ridders' method. Isotherms from the triple point temperature up to a sufficiently high temperature (see graphs) with small enough steps were investigated. To obtain isobaric extrema, we fixed the pressure and analyzed $X(T)$.

4. Results and discussion

Figures 1 to 4 show all studied loci in the $p-T$ (or, more precisely, p^*-T^*) plane. The three equations of state perform similarly for C_V^{res} and κ_T while important differences are observed for loci of isobaric extrema of α_p and isothermal and isobaric extrema of C_p^{res} . Results from PVE/hBH for the two former lines are similar to those reported by Stephenson (see, e.g., Ref. 5). This fact leads one to ascribe their nonregular, strange shapes as obtained from MBWR and vdW-LJ to numerical pitfalls. On recalling that all equations of state behave well for C_V^{res} and κ_T , one concludes that problems for these three types of lines originate from α_p . We must note that the situation for thermodynamic response functions contrasts with findings by Boshkova and Deiters for

the Amagat line, which evidence that vdW-LJ shows the best performance at low temperatures.

Symbols + and – in plots indicate the sign of derivatives with respect to pressure in the plots of isothermal extrema [(a) panels] or with respect to temperature in the plots of isobaric extrema [(b) panels]. Specifically, $(\partial C_V^{res} / \partial p)_T$ is negative inside the closed loops of Figure 1a, which correspond to isothermal extrema (maxima or minima) of C_V^{res} , and positive outside them. Analogously, loci of isobaric extrema of C_V^{res} in Figure 1b enclose regions of positive $(\partial C_V^{res} / \partial T)_p$ [with $(\partial C_V^{res} / \partial T)_p < 0$ outside the loops]. Consequent conclusions are obtained for $(\partial C_p^{res} / \partial p)_T$ in Figure 2a, $(\partial C_p^{res} / \partial T)_p$ in Figure 2b, $(\partial \alpha_p / \partial T)_p$ in Figure 3b, and $(\partial \kappa_T / \partial p)_T$ in Figure 4a. On the other hand, α_p just exhibits a locus of isothermal maxima, with $(\partial \alpha_p / \partial p)_T$ being positive below such line and negative in the remaining regions of the $p-T$ plane (see Figure 3a). And $(\partial \kappa_T / \partial T)_p$ is negative below lines of extrema in Figure 4b and positive otherwise. Clearly, to visualize the behavior of response functions, plots of isothermal extrema [(a) panels] must be seen “vertically” whereas those of isobaric extrema [(b) panels] must be analyzed “horizontally”. That is, on following, by way of example, a (super) near-critical isotherm in Figure 1a, one realizes that C_V^{res} increases with p at sufficiently high and low pressures and exhibits a maximum followed by a minimum in between; or, along a (super) near-critical isobar in Figure 1b, it is found that C_V^{res} decreases with T at sufficiently high and low temperatures and shows a minimum followed by a maximum in between.

At low enough pressures or high enough temperatures, the ideal-gas limit, namely, $C_V^{res}, C_p^{res} \rightarrow 0$, $\alpha_p \rightarrow 1/T$, and $\kappa_T \rightarrow 1/p$, is recovered. At high enough pressures or low enough temperatures, the structure of the system may correspond to that of a close-packed fluid. In such regions, C_p^{res} and C_V^{res} decrease with T and increase with p , α_p decreases with T and p , and κ_T increases with T and decreases with p . In some cases, the expected behavior at low temperatures and pressures is not seen for the stable liquid because of crystallization (see, e.g., the plot of isobaric extrema of α_p).

The pattern of behavior in the close-packed-fluid limit has been observed for molecular liquids at high pressures (primarily for $\alpha_p(T, p)$ data [25]) and ionic liquids at room temperature and atmospheric pressure [26-28]. That ionic liquids display wide liquid ranges with high critical temperatures [29] explains the observation of negative $(\partial\alpha_p/\partial T)_p$ and positive $(\partial C_p^{res}/\partial p)_T$ at ambient conditions [26]. Understandably, fluids of markedly different physicochemical nature behave similarly near close packing. The present results therefore cover behaviors beyond the LJ fluid.

In the liquid range, say, at subcritical pressures and temperatures not very far from the critical one so that fluctuations are non-negligible, C_V^{res} , C_p^{res} , α_p , and κ_T increase with T and decrease with p . Even in the case that temperature is far below T_c so that $(\partial C_V^{res}/\partial T)_p$ and $(\partial C_p^{res}/\partial T)_p$ are negative, $C_V = C_V^{ig} + C_V^{res}$ and $C_p = C_p^{ig} + C_p^{res}$ normally increase with T because C_V^{ig} and C_p^{ig} are increasing functions of T that usually dominate over the residual contribution.

1
2
3
4
5
6
7
8
9
10
11
12
13
14
15
16
17
18
19
20
21
22
23
24
25
26
27
28
29
30
31
32
33
34
35
36
37
38
39
40
41
42
43
44
45
46
47
48
49
50
51
52
53
54
55
56
57
58
59
60

At supercritical isobars or supercritical isotherms all properties show maxima that belong to loci emanating from the vapor-liquid critical point, where C_V^{res} , C_p^{res} , α_p , and κ_T diverge. In fact, though not shown here explicitly, asymptotically close to criticality all loci converge at the so-called Widom line (namely, the line of maxima of the correlation length), which has received considerable attention recently in connection with water's hypothetical second (liquid-liquid) critical point [30]. It is important to note, however, that maxima in thermodynamic response functions do not necessarily mark the proximity of criticality. Simulations on systems with no critical points, like one-dimensional fluids interacting via short-range pairwise interactions (including Lennard-Jones intermolecular potentials), reveal maxima in C_V^{res} [31]. As discussed previously [31,32], in going from the close-packed-fluid limit to the ideal-gas limit, energy fluctuations—which according to statistical mechanics contribute positively to C_V^{res} —inevitably result in $C_V^{res}(T)$ and $C_V^{res}(p)$ maxima.

5. Further remarks and outlook

We have shown that the analysis of loci of extrema of thermodynamic response functions in the $p-T$ plane is an adequate way of studying the global behavior of such properties. Results for the Lennard-Jones fluid may serve as a reference point: in view of what is known from experiments, we are led to think that it also qualitatively represents the behavior of many nonassociated molecular organic fluids, in accord with what Troncoso et al. [25] have recently found from their study for loci of extrema of α_p .

1
2
3
4
5
6 Association via hydrogen bonding gives rise to additional extrema. Indeed, it has
7
8 been shown [33] that energetic effects of hydrogen bonding in alcohols can give rise to
9
10 $C_V^{res}(T)$ and $C_p^{res}(T)$ maxima at atmospheric pressure and subcritical temperatures.
11
12 Therefore, at a (super) near-critical isobar C_V^{res} vs T and C_p^{res} vs T curves exhibiting two
13
14 maxima are expected for these fluids. And in certain specific cases such behavior can
15
16 also be found for total heat capacities: a $C_p(T)$ maximum arising from association effects
17
18 has been observed experimentally for branched alcohols [33,34]. It seems therefore
19
20 natural to extend the present analysis to associated fluids with the aid of specific EoS
21
22 (see, for instance, Refs. 35-39).
23
24
25
26
27

28 Water represents a case of study of extreme complexity because of its anomalous
29
30 thermodynamics at low temperatures, down to the deeply supercooled regime [40]. The
31
32 hypothetical existence of a liquid-liquid critical point in such region [40] may result in
33
34 heat-capacity and κ_T maxima as well as in α_p minima (since α_p is expected to diverge
35
36 to $-\infty$ at that critical point). Even in the so-called singularity-free scenario [41], where
37
38 anomalies are explained without any appeal to a second critical point, loci of extrema are
39
40 present [41,42]. Certainly, tracing out loci of extrema for water's EoS should reveal the
41
42 richest phenomenology among common organic fluids.
43
44
45
46
47
48
49

50 Acknowledgements

51
52 Financial support from "Consellería de Educación e Ordenación Universitaria (Xunta de
53
54 Galicia)" and "Ministerio de Ciencia e Innovación" of Spain (#FIS2009-07923) is
55
56 gratefully acknowledged. Research of P.T-A. was supported by "Consejo Nacional de
57
58 Ciencia y Tecnología CONACyT" of Mexico.
59
60

References

- [1] J.S. Rowlinson, Rep. Prog. Phys. **28**, 169 (1965).
- [2] E.H. Brown, Bulletin Inst. Ind. de Froid Annexe (International Institute of Refrigeration, 1960-1), pp. 169.
- [3] O.L. Boshkova and U.K. Deiters, Int. J. Thermophys. **31**, 227 (2010).
- [4] J. Gregorowicz, J.P. O'Connell, and C.J. Peters, Fluid Phase Equilib. **116**, 94 (1996).
- [5] J. Stephenson, Phys. Chem. Liq. **8**, 235 (1979).
- [6] J. Stephenson and H.K. Leung, Phys. Chem. Liq. **8**, 249 (1979).
- [7] J. Stephenson, Phys. Chem. Liq. **8**, 265 (1979).
- [8] J. Stephenson, Phys. Chem. Liq. **9**, 23 (1979).
- [9] J. Stephenson, Phys. Chem. Liq. **9**, 37 (1979).
- [10] J. Stephenson, Phys. Chem. Liq. **9**, 51 (1979).
- [11] J. Stephenson, Phys. Chem. Liq. **9**, 175 (1980).
- [12] J. Stephenson, Phys. Chem. Liq. **10**, 153 (1980).
- [13] J. Stephenson and R. Couzens, Phys. Chem. Liq. **10**, 167 (1980).
- [14] J. Stephenson, Phys. Chem. Liq. **10**, 229 (1981).
- [15] J.K. Johnson, J.A. Zollweg, and K.E. Gubbins, Mol. Phys. **78**, 591 (1993).
- [16] J. Kolafa and I. Nezbeda, Fluid Phase Equilib. **100**, 1 (1994).
- [17] M. Mecke, A. Müller, J. Winkelmann, J. Vrabec, J. Fischer, R. Span, and W. Wagner, Int. J. Thermophys. **17**, 391 (1996).
- [18] J.J. Nicolas, K.E. Gubbins, W.B. Streett, and D.J. Tildesley, Mol. Phys. **37**, 1429 (1979).

- 1
2
3
4
5
6 [19] T. Boublík and I. Nezbeda, *Collec. Czech. Chem. Commun.* **51**, 2301 (1986).
7
8
9 [20] N.F. Carnahan and K.E. Starling, *J. Chem. Phys.* **51**, 635 (1969).
10
11 [21] B. Saager, R. Hennenberg, and J. Fischer, *Fluid Phase Equilib.* **72**, 41 (1992).
12
13 [22] M. Mecke, A. Müller, J. Winkelmann, J. Vrabec, J. Fischer, R. Span, and W.
14
15 Wagner, *Int. J. Thermophys.* **19**, 1493 (1998).
16
17 [23] W.H. Press, S.A. Teulolsky, W.T., Vetterling, B.P. Flannery, *Numerical Recipes in*
18
19 *Fortran 77*, second edition (Cambridge University Press, Cambridge, UK, 1992), pp. 180-
20
21 184.
22
23 [24] E.A. Mastny and J.J. de Pablo, *J. Chem. Phys.* **127**, 104504 (2007).
24
25 [25] J. Troncoso, P. Navia, L. Romani, D. Bessieres, and T. Lafitte, *J. Chem. Phys.* **134**,
26
27 097502 (2011).
28
29 [26] J. Troncoso, C.A. Cerdeiriña, P. Navia, Y.A. Sanmamed, D. González-Salgado, and
30
31 L. Romani, *J. Phys. Chem. Lett.* **1**, 211 (2010).
32
33 [27] P. Navia, J. Troncoso, and L. Romani, *J. Chem. Eng. Data* **55**, 595 (2010).
34
35 [28] Y.A. Sanmamed, P. Navia, D. González-Salgado, J. Troncoso, and L. Romani, *J.*
36
37 *Chem. Eng. Data* **55**, 600 (2010).
38
39 [29] L.P.N. Rebelo, J.N.C. Lopes, J.M.S.S. Esperança, and E. Filipe, *J. Phys. Chem. B*
40
41 **109**, 6040 (2005).
42
43 [30] G. Franzese and H.E. Stanley, *J. Phys.: Condens. Matter* **19**, 205126 (2007).
44
45 [31] B.C. Freasier, C.E. Woodward, and R.J. Bearman, *J. Chem. Phys.* **106**, 10318
46
47 (1997).
48
49 [32] M.M. Piñeiro, C.A. Cerdeiriña, and M. Medeiros, *J. Chem. Phys.* **129**, 014511
50
51 (2008).
52
53
54
55
56
57
58
59
60

- 1
2
3
4
5
6 [33] C.A. Cerdeiriña, D. González-Salgado, L. Romaní, M.C. Delgado, L.A. Torres, and
7
8 M. Costas, *J. Chem. Phys.* **120**, 6648 (2004).
9
- 10 [34] C.A. Cerdeiriña, J. Troncoso, D. González-Salgado, G. García-Miaja, G.O.
11
12 Hernández-Segura, D. Bessieres, M. Medeiros, L. Romaní, and M. Costas, *J. Phys.*
13
14 *Chem. B* **111**, 1119 (2007).
15
- 16 [35] F. Llovel and L.F. Vega, *J. Phys. Chem. B* **110**, 11427 (2006).
17
- 18 [36] T. Lafitte, D. Bessieres, M.M. Piñeiro, and J.-L. Daridon, *J. Chem. Phys.* **124**,
19
20 024509 (2006).
21
22
- 23 [37] T. Lafitte, M.M. Piñeiro, J.-L. Daridon, and D. Bessieres, *J. Phys. Chem. B* **111**,
24
25 3447 (2007).
26
27
- 28 [38] M. Medeiros and P. Téllez-Arredondo, *Ind. Eng. Chem. Res.* **47**, 5723 (2008).
29
- 30 [39] R. Reynoso-López, P. Téllez-Arredondo, and M. Medeiros, *Fluid Phase Equilib.*
31
32 **297**, 98 (2010).
33
34
- 35 [40] P.G. Debenedetti, *J. Phys.: Condens. Matter* **15**, R1669 (2003).
36
37
- 38 [41] S. Sastry, P.G. Debenedetti, F. Sciortino, and H.E. Stanley, *Phys. Rev. E* **53**, 6144
39
40 (1996).
41
42
- 43 [42] L. P. N. Rebelo, P.G. Debenedetti, and S. Sastry, *J. Chem. Phys.* **109**, 626 (1998).
44
45
46
47
48
49
50
51
52
53
54
55
56
57
58
59
60

1
2
3
4
5
6
7
8
9
10
11
12
13
14
15
16
17
18
19
20
21
22
23
24
25
26
27
28
29
30
31
32
33
34
35
36
37
38
39
40
41
42
43
44
45
46
47
48
49
50
51
52
53
54
55
56
57
58
59
60

FIGURE CAPTIONS

Figure 1. Loci of extrema for the residual isochoric heat capacity C_V^{res} of the Lennard-Jones fluid from MBWR (A), PVE/hBH (B), and LJ-vdW (C) equations of state. Lines in (a) correspond to isothermal extrema, which, as indicated explicitly, divide the p^*-T^* plane into regions of different sign of $(\partial C_V^{res} / \partial p)_T$; lines in (b) correspond to isobaric extrema, which delimitate regions of different sign of $(\partial C_V^{res} / \partial T)_p$. (—) maxima; (···) minima. Data for the phase equilibrium lines were taken from Refs. 15-17 (liquid-gas) and Ref. 24 (solid-liquid). As defined in Section 2, $p^* \equiv p\sigma^3 / \varepsilon$ and $T^* \equiv Tk_B / \varepsilon$.

Figure 2. Loci of extrema for the residual isobaric heat capacity C_p^{res} of the Lennard-Jones fluid from MBWR (A), PVE/hBH (B), and LJ-vdW (C) equations of state. Lines in (a) correspond to isothermal extrema, which, as indicated explicitly, divide the p^*-T^* plane into regions of different sign of $(\partial C_p^{res} / \partial p)_T$; lines in (b) correspond to isobaric extrema, which delimitate regions of different sign of $(\partial C_p^{res} / \partial T)_p$. (—) maxima; (···) minima. Data for the phase equilibrium lines were taken from Refs. 15-17 (liquid-gas) and Ref. 24 (solid-liquid). As defined in Section 2, $p^* \equiv p\sigma^3 / \varepsilon$ and $T^* \equiv Tk_B / \varepsilon$.

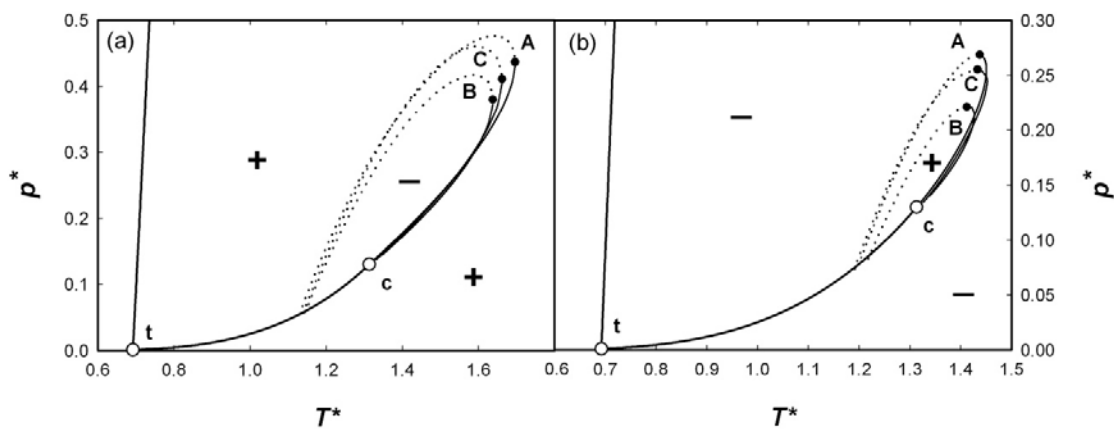
Figure 3. Loci of extrema for the isobaric thermal expansivity α_p of the Lennard-Jones fluid from MBWR (A), PVE/hBH (B), and LJ-vdW (C) equations of state. Lines in (a) correspond to isothermal extrema, which, as indicated explicitly, divide the p^*-T^*

1
2
3
4
5
6 plane into regions of different sign of $(\partial\alpha_p/\partial p)_T$; lines in (b) correspond to isobaric
7
8
9 extrema, which delimitate regions of different sign of $(\partial\alpha_p/\partial T)_p$. (—) maxima; (⋯)
10
11 minima. Data for the phase equilibrium lines were taken from Refs. 15-17 (liquid-gas)
12
13 and Ref. 24 (solid-liquid). As defined in Section 2, $p^* \equiv p\sigma^3/\varepsilon$ and $T^* \equiv Tk_B/\varepsilon$.
14
15
16

17
18
19 Figure 4. Loci of extrema for the isothermal compressibility κ_T of the Lennard-Jones
20
21 fluid from MBWR (A), PVE/hBH (B), and LJ-vdW (C) equations of state. Lines in (a)
22
23 correspond to isothermal extrema, which, as indicated explicitly, divide the p^*-T^*
24
25 plane into regions of different sign of $(\partial\kappa_T/\partial p)_T$; lines in (b) correspond to isobaric
26
27 extrema, which delimitate regions of different sign of $(\partial\kappa_T/\partial T)_p$. (—) maxima; (⋯)
28
29 minima. Data for the phase equilibrium lines were taken from Refs. 15-17 (liquid-gas)
30
31 and Ref. 24 (solid-liquid). As defined in Section 2, $p^* \equiv p\sigma^3/\varepsilon$ and $T^* \equiv Tk_B/\varepsilon$.
32
33
34
35
36
37
38
39
40
41
42
43
44
45
46
47
48
49
50
51
52
53
54
55
56
57
58
59
60

1
2
3
4
5
6
7
8
9
10
11
12
13
14
15
16
17
18
19
20
21
22
23
24
25
26
27
28
29
30
31
32
33
34
35
36
37
38
39
40
41
42
43
44
45
46
47
48
49
50
51
52
53
54
55
56
57
58
59
60

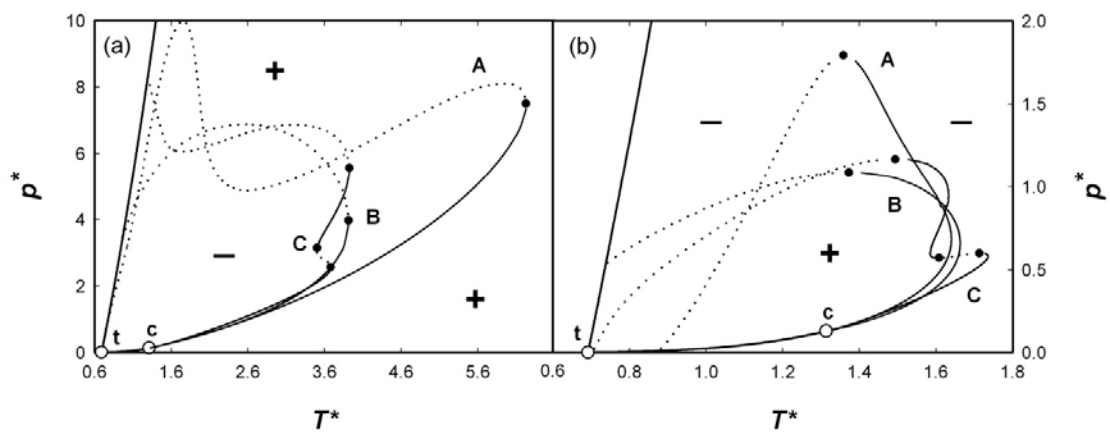
Figure 1



1
2
3
4
5
6
7
8
9
10
11
12
13
14
15
16
17
18
19
20
21
22
23
24
25
26
27
28
29
30
31
32
33
34
35
36
37
38
39
40
41
42
43
44
45
46
47
48
49
50
51
52
53
54
55
56
57
58
59
60

For P

Figure 2



W Only

1
2
3
4
5
6
7
8
9
10
11
12
13
14
15
16
17
18
19
20
21
22
23
24
25
26
27
28
29
30
31
32
33
34
35
36
37
38
39
40
41
42
43
44
45
46
47
48
49
50
51
52
53
54
55
56
57
58
59
60

Figure 3

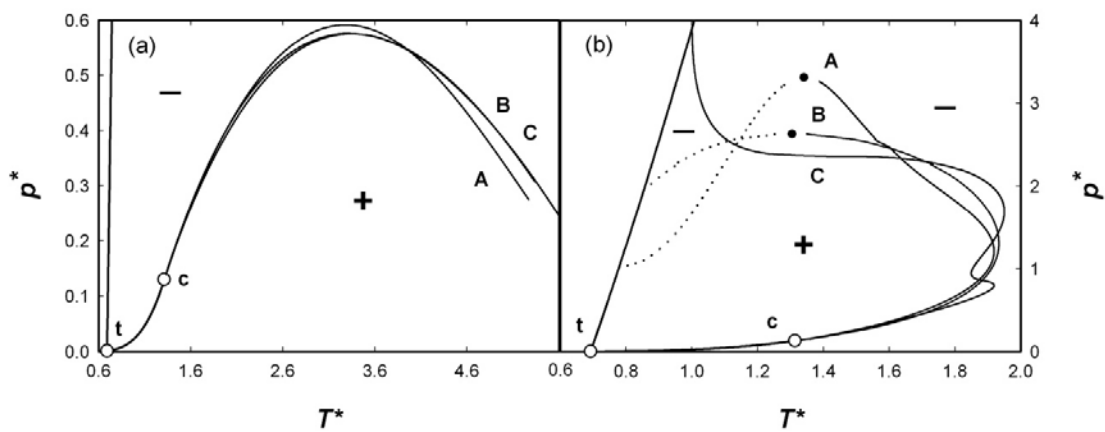


Figure 4

